Cell PRESS
Structure
Article

A Potent Peptidomimetic Inhibitor of Botulinum Neurotoxin Serotype A Has a Very Different Conformation than SNAP-25 Substrate

Jorge E. Zuniga,[1] James J. Schmidt,[2] Timothy Fenn,[1] James C. Burnett,[3] Demet Araç,[1] Rick Gussio,[4] Robert G. Stafford,[2] Shirin S. Badie,[2] Sina Bavari,[2] and Axel T. Brunger[1,*]
[1]Howard Hughes Medical Institute and Departments of Molecular and Cellular Physiology, Neurology and Neurological Science, Structural Biology, and Photon Science, Stanford University, Stanford, CA 94305, USA
[2]United States Army Medical Research Institute of Infectious Diseases, Fort Detrick, Frederick, MD 21702, USA
[3]Target Structure-Based Drug Discovery Group, SAIC-Frederick, Inc.
[4]Developmental Therapeutics Program
National Cancer Institute, Frederick, MD 21702, USA
*Correspondence: brunger@stanford.edu
DOI 10.1016/j.str.2008.07.011

SUMMARY

Botulinum neurotoxin serotype A is the most lethal of all known toxins. Here, we report the crystal structure, along with SAR data, of the zinc metalloprotease domain of BoNT/A bound to a potent peptidomimetic inhibitor (K_i = 41 nM) that resembles the local sequence of the SNAP-25 substrate. Surprisingly, the inhibitor adopts a helical conformation around the cleavage site, in contrast to the extended conformation of the native substrate. The backbone of the inhibitor's P1 residue displaces the putative catalytic water molecule and concomitantly interacts with the "proton shuttle" E224. This mechanism of inhibition is aided by residue contacts in the conserved S1′ pocket of the substrate binding cleft and by the induction of new hydrophobic pockets, which are not present in the apo form, especially for the P2′ residue of the inhibitor. Our inhibitor is specific for BoNT/A as it does not inhibit other BoNT serotypes or thermolysin.

INTRODUCTION

Neurotoxins produced by the genus *Clostridium* are potent chemodenervating zinc-dependent proteases that prevent the Ca^{2+}-triggered release of acetylcholine in neuromuscular junctions by cleaving one of three SNARE proteins (Schiavo et al., 1992; Blasi et al., 1993a, 1993b). Hydrolysis of these target proteins renders them noncompetent for facilitating the membrane fusion step that takes place before acetylcholine release in the synaptic cleft. Because their use as therapeutic and cosmetic agents has become increasingly widespread, a concomitant increased risk of accidental overdosing can be expected. In addition, since botulinum neurotoxins (BoNTs) can be easily produced and delivered via aerosol medium, these agents are considered to be among the most deadly of all potential bioweapons (Josko, 2004). Therefore, the need for potent and effective inhibitors is a high priority. In this regard, peptidomimetics and hydroxamic acid-based inhibitors have been developed that display inhibitory effects in the high nM range for the light chain of the BoNT serotype A (BoNT/A LC) (Boldt et al., 2006; Burnett et al., 2007; Kumaran et al., 2008; Silvaggi et al., 2008). Compounds that contain zinc-coordinating sulfhydryl moieties might potentially inhibit host zinc proteases thereby making them poor therapeutic leads. The characteristically poor pharmacokinetics of hydroxamates, their instability, and their reported toxicity, which is likely due to their inhibition of an array of metalloproteases, also make them problematic as therapeutic agents (Rao, 2005; Suzuki and Miyata, 2005).

In this study, we report the crystal structure of a tight complex between an active form of BoNT/A LC and a pseudopeptide inhibitor that mimics the 7-residue QRATKML sequence of the 206-residue SNAP-25, the natural substrate of the BoNT/A LC (Blasi et al., 1993a), near the cleavage site (Figures 1A and 1B). This inhibitor, referred herein as I1, is the most potent non-zinc-chelating, non-hydroxamate-based antagonist reported to date, with a K_i = 41 nM. When tested against serotypes B, D, E, F, and thermolysin, I1 did not display any detectable inhibition in our assays, indicating that its inhibitory action is BoNT/A specific. Our structure reveals a 3_{10} helical backbone conformation for the peptide inhibitor bound to the active site of BoNT/A LC. This is in sharp contrast to the extended conformation of bound SNAP-25 observed in the BoNT/A LC[E224Q,Y366F]:SNAP-25 complex (Breidenbach and Brunger, 2004). The inhibitor induces binding pockets in BoNT/A LC that are not found in either the apo BoNT/A LC or the BoNT/A LC[E224Q,Y366F]:SNAP-25 complex. The information gained from these new, induced pockets, together with additional binding surfaces identified in the vicinity of the I1-binding sites, will be useful for the development of efficacious antibotulinum drugs.

RESULTS AND DISCUSSION

The crystal structures of both free and I1-bound wild-type BoNT/A LCs were determined by molecular replacement (see Table 1 and Experimental Procedures). All seven residues of the I1 inhibitor could be readily assigned on the basis of the highly interpretable, observed difference electron-density map (Figure 1C). The

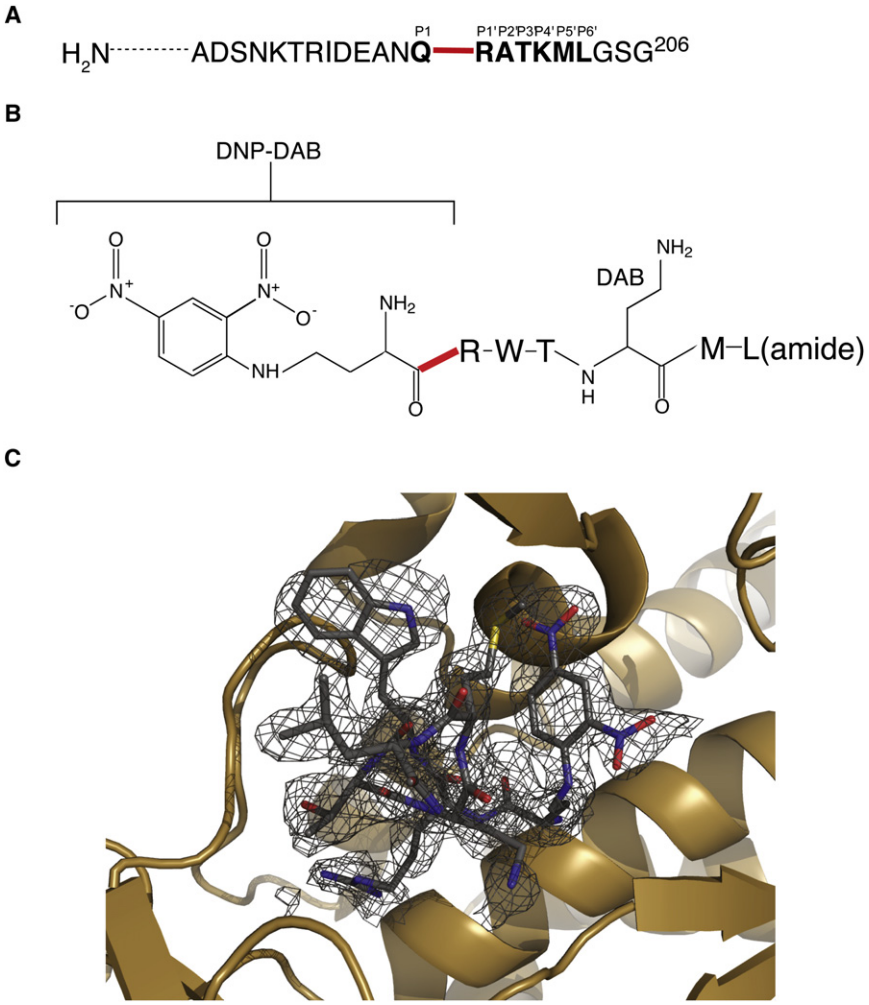

Figure 1. Two-Dimensional Structure and Electron Density for I1

(A) One-letter code sequence for the 22 C-terminal residues of the human SNAP-25 consisting of 206 residues. The 7-residue peptide sequence (Q197-L203) of SNAP-25 used to design I1 and its variants is shown in bold, and their corresponding positions in the inhibitor indicated as P1-P6′. The amino terminus is indicated.

(B) Schematic representation of the I1 inhibitor. Residues Q197, A199, and K201 in the Q197-L203 peptide have been replaced by DNP-DAB, Trp, and DAB, respectively. DNP-DAB: 4-(2,4-dinitrophenylamino)-2-amino-butanoic acid; DAB: 2,4-diaminobutanoic acid. In both panels, the scissile peptide bond is indicated by a thick, red line.

(C) View of a σ_A-weighted F_o-F_c electron-density map contoured at 1.8σ (gray mesh) around I1 overlaid with the refined model of the complex (I1 in gray sticks and BoNT/A LC in tan ribbon representation). This map was computed with phases calculated prior to the inclusion of the I1 inhibitor (i.e., it is a model-bias free map).

overall architecture, secondary structural elements, as well as the conformation of the zinc-coordinating residues in the active site of I1-bound BoNT/A LC, remain essentially unaltered relative to the apo form of the protease crystallized under the same conditions. This is indicated by an RMSD of 0.83 Å over all α carbons of both structures of the enzyme, as well as by comparisons to other reported BoNT/A LC structures (Figure 2).Nonetheless, binding of I1 is accompanied by significant conformational changes in the 60, 250, and 370 loops, confirming an observation that the BoNT/A LC active site has a high degree of "plasticity," as proposed previously (Kukreja and Singh, 2005; Burnett et al., 2007; Silvaggi et al., 2007). With respect to bound I1, the P2′-P5′ residues adopt a compact, 3_{10} helical conformation, with the backbone oriented such that its analogous scissile bond (i.e., the bond between the P1-P1′ residues) is buried deep within the active site, close to the zinc ion. The remainder of the inhibitor backbone chain orients toward the solvent-exposed surface of the protease (Figure 3A).

Binding Determinants in the BoNT/A LC:I1 Complex

Our structure reveals that I1 induces conformational changes in the active site of BoNT/A LC upon binding, as detailed below. Strikingly, when the apoenzyme and I1-bound BoNT/A LC structures are superimposed, steric clashes are readily observed between the Trp, Thr, and Leu residues of the inhibitor (positions P2′, P3′, and P6′, respectively) and their complementary apoenzyme residues (Figure 4).

The observed induced fit rationalizes the relatively high affinity of I1 (K_i = 41 nM; Table 2), especially when interpreted in context with inhibition data from inhibitor variants. To exemplify, the polar nitro and butanoic acid groups on the inhibitor's aromatic P1 residue stabilizes a network of hydrogen bonds with solvent and the backbone amide group of the BoNT/A LC residue S259 (Figure 3B). The presence of these stabilizing hydrogen bonds is consistent with the observation that a Phe, Gln, or Gly in this position (Table 2; peptides I6, I2, and I7, respectively) results in decreased inhibition (K_i values of 8.3, 6.5, and 3.3 μM, respectively). Specifically, these peptides lack the isosteric polarity of the 4-(2,4-dinitrophenylamino)-2-diamino-butanoic acid (DNP-DAB) group (Table 2; peptides I8 and I1 with K_i values of 0.98 and 0.041 μM, respectively) and, hence, the ability to make critical polar/ionic interactions with solvent and BoNT/A LC residue S259.

The P1′ residue of I1 establishes a critical anchoring neighboring point in the BoNT/A LC binding cleft. The side chain of P1′ Arg is projected into a deep pocket of the cleft (Figure 3C), where it engages in a salt bridge with the side chain of D370. For this interaction to be possible, the 370 loop of BoNT/A LC undergoes a major conformational rearrangement such that the side chain of D370, which is solvent exposed in the apo form, reorients into the active site. This reorientation is stabilized by a hydrogen bond between the side chain hydroxyl group of the I1 P3′ Thr residue and the carboxylate group of BoNT/A LC D370, while the guanidinium group of I1 P1′ Arg is also in close proximity to the aromatic ring of BoNT/A LC F194, suggesting that cation-π

Table 1. X-Ray Data Collection and Refinement

Crystallographic Data		
	BoNT/A LC	BoNT/A LC:I1
Space group	$P2_12_12$	$P2_12_12$
a, *b*, *c* (Å)	56.8, 191.1, 42.1	58.8, 189.2, 42.3
Resolution (Å)	45–1.9 (1.98–1.90)	36–1.9 (1.98–1.90)
Unique reflections	46184	42358
Redundancy	4.2 (3.6)	5.9 (5.8)
Completeness (%)	95.9 (95.1)	76.1 (88.1)
I/σ	17.1 (1.3)	14.9 (2.8)
R_{sym}[a] (%)	9.5% (95.8%)	10.1% (53%)
Refinement		
	BoNT/A LC	BoNT/A LC:I1
Resolution (Å)	45–1.9	36–1.9
R_{cryst}/R_{free}[b,c]	18.0% / 24.3%	21.2% / 24.7%
No. atoms		
BoNT/A LC	3196	3225
I1	Na	75
Ni	1	1
Zn	1	1
Water	250	232
Average thermal (B) factor		
BoNT/A LC	29.2 Å^2	26.7 Å^2
I1	Na	27.9 Å^2
Ni	20.3 Å^2	23.9 Å^2
Zn	18.4 Å^2	18.2 Å^2
Water	37.7 Å^2	32.3 Å^2
Rmsds		
Average bond length deviation	0.004 Å	0.007 Å
Average bond angle deviation	0.84°	1.0°

Values in parentheses are for the high-resolution bin.
[a] $R_{sym} = \sum_h\sum_i|I_i(h) - < I(h) > |/\sum_h\sum_i I_i(h)$, where $I_i(h)$ is the i^{th} measurement and $< I(h) >$ is the mean of all measurements of I(h) for Miller indices h.
[b] $R_{cryst} = \sum||F_{obs}| - k|F_{calc}||/\sum|F_{obs}|$
[c] Free R value is the R value obtained for a test set of reflection (5% of total) not used during refinement.

interactions may further stabilize this orientation. Interestingly, a similar binding mode has been reported for an arginine hydroxamate (Arg-HX) inhibitor in complex with BoNT/A LC (Silvaggi et al., 2007).

A second, extensive anchoring contact that enhances the binding of I1 to the active site is the P2′ Trp, which docks to an induced hydrophobic pocket composed of side chains V245, L256, V258, Y366, L367, and F369, with the latter oriented such that aromatic ring π-stacking is facilitated (Figure 3D). In addition, the Trp indole ring nitrogen forms a hydrogen bond with the backbone carbonyl of E257. In this pocket, the side chain of F369 is repositioned relative to the apo form of BoNT/A LC, which is accompanied by a conformational change of the 370 loop. In addition, residue L367 is displaced to accommodate the I1 Trp side chain. Taken together, this induced fit to I1's steric and chemical complementarity may signify the existence of a structural "Achilles tendon" in the BoNT/A LC protease, suggesting a diversity of strategies for structure-based inhibitor development by making use of new induced pockets in the active site.

The binding mode for P2′ Trp provides a qualitative explanation for the weaker inhibitory potencies of related pseudopeptide derivatives. In particular, when the wild-type SNAP-25 Ala is present in the P2′ position (Table 2; peptide I8), the K_i is increased by a factor of 25 relative to I1. This can be attributed to reduced favorable hydrophobic interactions with the smaller methyl group. Similarly, with I11, a Phe residue in this position is also not as favorable as Trp, indicated by only an 8-fold increase in K_i, compared with I1. It might be argued that a fraction of these reductions can be attributed to the Lys substitution in position P4′, but this substitution has only a minor effect on inhibitory activity (K_i increase of ~2.5 fold relative to I1). We estimated the effect of the Lys substitution by comparing peptides I9 and I10 and from the observation that a BZA substitution in position P2′ has no statistically significant effect on K_i (compare I1 and I10).

The P2′ Trp also induces a pocket for the adjacent P3′ Thr of I1. Specifically, the P3′ Thr side chain points into the substrate-binding cleft, where its hydroxyl moiety engages in a hydrogen bond with the D370 side chain carboxylate (Figure 3C), and its methyl group makes hydrophobic contacts with the V70 side chain.

Of further importance for the affinity of I1 are the P4′ 2,4-diaminobutanoic acid (DAB) contacts with BoNT/A LC, and intrapeptide contacts with the methylenes of P1 DNP-DAB (Figure 3E). The free terminal 4-amino substituent engages in a hydrogen bond with the side chain carboxyl oxygen of Q162. This interaction provides structure-based explanations for the inhibition data of similar analogs (Table 2). In one example, increasing the length of the DAB side chain by a longer ornithine side chain is sterically unfavorable, resulting in a 2-fold decrease in inhibition (Table 2; peptide I12). Likewise, the structure suggests why decreasing the DAB side chain length decreases inhibition. This is exemplified in the 2,3-diaminopropanoic acid (DAP) derivative that possesses a K_i that is one order of magnitude larger than that of I1 (see Table 2; derivative I13). This decreased inhibition can be explained by the lost hydrogen bond with Q162 (Figure 3E).

Unlike most other residue positions in I1, the P5′ Met only engages in intrapeptide binding contacts (Figure 3A). Specifically, this residue stabilizes the intramolecular hydrophobic collapse of the aromatic ring of the P1 DNP-DAB. The Leu in position P6′ induces a conformational change in the 60 loop (Figure 4). In particular, the side chain of residue R66 is slightly displaced relative to its position in the apoenzyme, relieving steric clashes with the terminal carboxyl group and electrostatic repulsions with the synthetically added C-terminal amide of this residue.

Inhibition Mechanism

The mechanism for peptide cleavage employed by the BoNT/A LC is believed to be similar to that of thermolysin, as supported by several structural and mutagenesis studies (Li et al., 2000; Binz et al., 2002; Agarwal et al., 2004; Swaminathan et al., 2004) (Figures 5A–C). In this model, the geometry of the zinc ion coordination in the active site changes upon SNAP-25 binding, such that the catalytic water is displaced by the carbonyl oxygen in the P1 position (i.e., Q197) of the substrate and placed in proximity to the carboxylate group of the putative "proton shuttle," E224 (Figure 5A). As a result, the catalytic water makes two

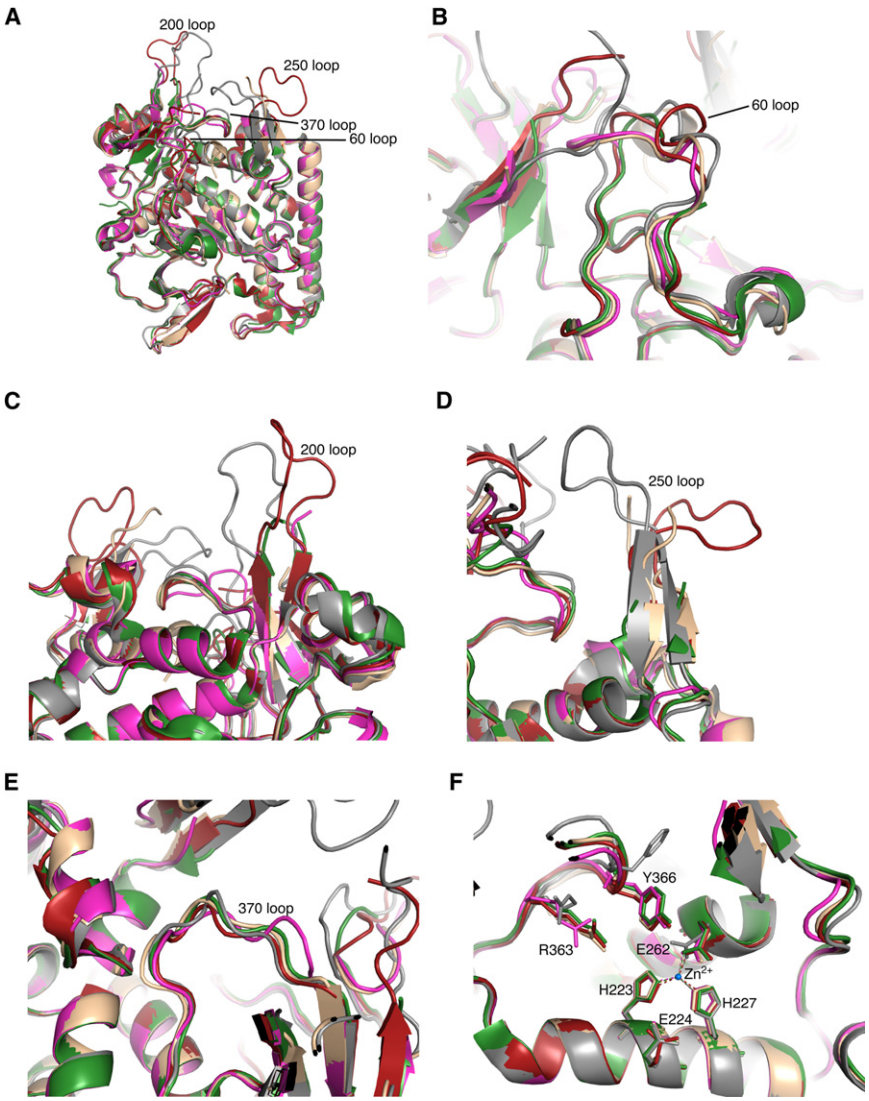

Figure 2. Superposition of BoNT/A Crystal Structures

(A) Comparison of the backbone trace of reported crystal structures of BoNT/A LC. The apo form of wild-type BoNT/A obtained in the presence of $NiCl_2$ is colored magenta; wild-type BoNT/A LC in complex with I1 is colored tan; the apo form of the wild-type BoNT/A LC obtained in the absence of $NiCl_2$ is colored red (Burnett et al., 2007) (PDB ID: 2ISE); the SNAP-25-bound form of the E224Q/Y366F BoNT/A LC is colored gray (Breidenbach and Brunger, 2004) (PDB ID: 1XTG); the ArgHX-bound form of the wild-type BoNT/A LC is colored green (Silvaggi et al., 2007) (PDB ID: 2IMB). Flexible loops are labeled.

(B–E) Enlargements of the superposition of the 60, 200, 250, and 350 loops, respectively.

(F) Superposition of the zinc-coordinating residues (sticks) as well as R363 and Y366 in all five structures indicated above.

H-bonds with E224 in a bidentate manner. From this position, the oxygen atom in the catalytic water remains weakly coordinated to the zinc, resulting in the penta-coordination of the metal ion. Hence, E224 acts as a general base to generate a hydroxide ion that is oriented for nucleophilic attack on the carbonyl carbon of the scissile peptide bond (Figure 5B). This tetrahedral intermediate state is stabilized by putative interactions provided by the zinc ion and the hydroxyl group of Y366. Finally, the collapse of this tetrahedral intermediate and the E224-mediated transfer of two protons onto the scissile amide generate a stable amino group that then leaves the active site (Figure 5C). In this model, the catalytic water, together with the proton shuttle E224, are of critical importance for catalytic hydrolysis of the peptide bond in the SNAP-25 substrate.

Consistent with this model, the structure of the BoNT/A LC:I1 complex shows that the carbonyl oxygen of P1 DNP-DAB is indeed acting as the fourth zinc-coordinating group in the complex, instead of the catalytic water molecule (Lacy et al., 1998), a feature that has been previously reported for small molecule hydroxamate inhibitors in complex with the BoNT/A LC (Fu et al., 2006; Silvaggi et al., 2007) (Figure 5D; Figure 6). In addition, the complex structure also confirms the proposed hydrogen bonding between the hydroxyl group of the Y366 side chain in the BoNT/A LC, and the P1 carbonyl oxygen (Figures 3B and 5D). Nonetheless, the P1 N-terminal amino group forms a hydrogen bond with the carboxylate group of E224, the putative proton shuttle residue in the BoNT/A LC (Li et al., 2000), effectively abrogating any interaction between E224 and a potential catalytic water molecule (Figures 3B, 5D, and 6). Thus, E224 is clearly not positioned for a potential nucleophilic attack on the scissile carbonyl. In addition to this proton shuttle "blocking" effect, the putative scissile amide in position P1′ in the inhibitor is distant from the E224 carboxylate group, further hampering any hydrolytic event with the scissile bond. Consistent with this inhibitory role for the N-terminal amino group in I1, similar pseudopeptide derivatives, in which the amino group in question has been eliminated, acetylated or configurationally reoriented so that it cannot engage in this hydrogen bond (Table 2; peptides I3, I4, and I5, respectively), show less inhibition than the corresponding derivatives with a free amino group (e.g., peptides I2 and I1).

The interactions observed for residues P1′-P3′ stabilize the orientation of the backbone of residue P1 for inhibition at the active site. Presumably, the binding mode of this P1′-P3′ peptide segment would orient the backbone of any residue bearing a free amino group (as explained above) in the P1 position so as to achieve the inhibitory mode observed for DNP-DAB in I1—that is, by occupying the position of the catalytic water. *In silico* mutation of the DNP-DAB residue in the complex structure suggests that the backbone of a Gln residue in this position would also be placed in the same inhibitory mode described for DNP-DAB (not shown). In agreement with our model, a 7-residue

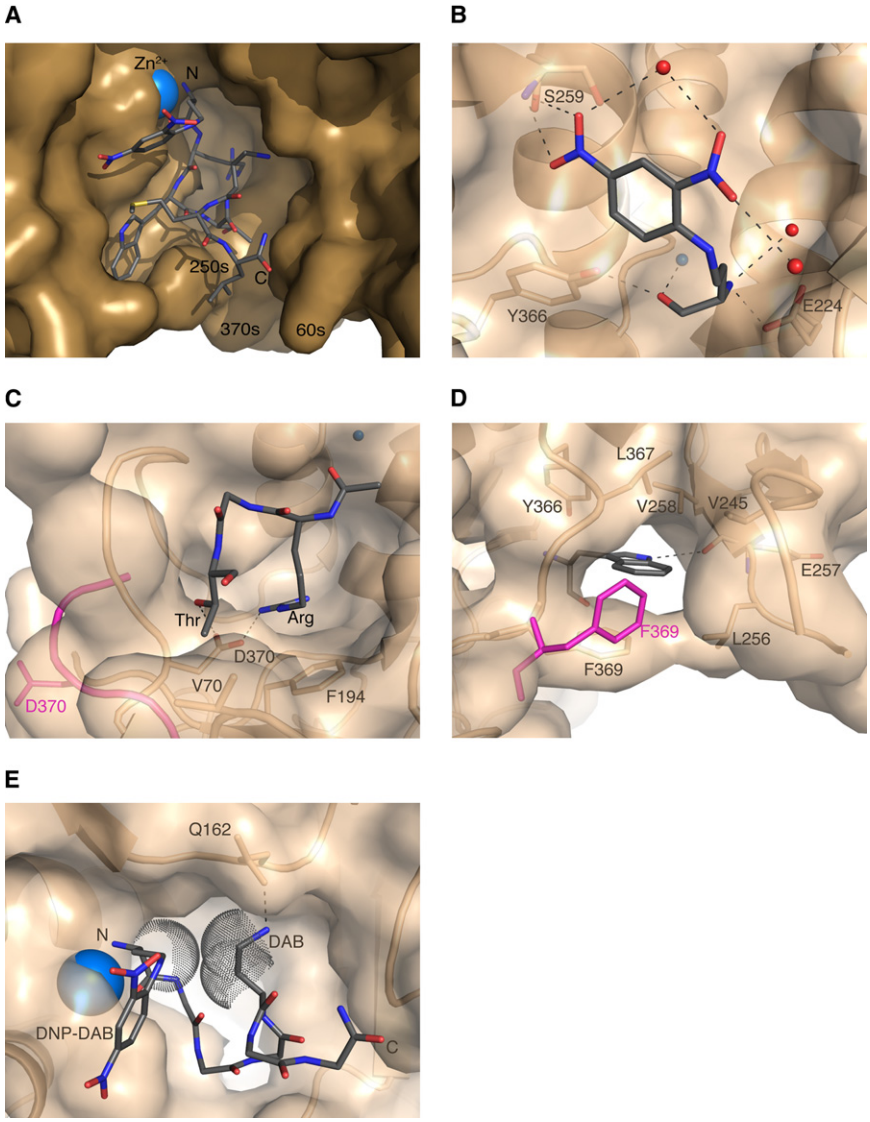

Figure 3. Interactions of I1 with BoNT/A LC

(A) Complex of I1 (sticks) with BoNT/A LC (gold surface). The N and C termini of I1, as well as the 60, 250, and 370 loops are labeled.

(B) Interactions of I1 residue P1 with BoNT/A LC (tan), water molecules (red spheres), and the zinc ion.

(C) Interactions of the P1′ (Arg) and P3′ (Thr) residues of I1 with BoNT/LC (tan). Superimposed is residue D370 of the apo form of the BoNT/A LC (magenta).

(D) Interactions of I1 residue P2′ (Trp) with BoNT/A LC (tan). Superimposed is residue F369 of the apo form of BoNT/A LC (magenta).

(E) Interactions of I1 residue P4′ (DAB) with BoNT/A LC and with residue P1 (DNP-DAB) of I1. Van der Waals interactions between DNP-DAB and DAB side chain methylene groups are displayed as gray dots. The N and C termini of the I1 inhibitor are indicated by N and C, respectively.

In all panels, selected hydrogen bonds between the protease and inhibitor residues are indicated by gray dashes. C, N, and O atoms of I1 are color-coded in the stick representations (gray, blue, and red, respectively). Where shown, the zinc ion is displayed as a blue sphere.

peptide containing the wild-type sequence of the SNAP-25 substrate (and, therefore, the Gln-Arg scissile peptide bond), showed inhibitory activity with no detectable hydrolysis (see Table 2; peptide I2), reinforcing the notion that the residue at the P1 position of all inhibitors in Table 2 deactivates BoNT/A LC by displacing the nucleophilic water and simultaneously "locking" the E224 proton shuttle.

To assess whether the inhibitory mechanism of I1 is specific for BoNT/A LC, we examined it against four other BoNT serotypes, as well as against thermolysin. When BoNT serotypes B, D, E, and F or thermolysin were incubated with hydrolyzable constructs of their respective substrates, the presence of I1 did not have any inhibitory effects on the cleavage of these substrates (Table 3). Thus, I1 is a highly specific inhibitor for the BoNT/A LC.

The I1 and SNAP-25 Binding Modes Differ

Normally, one might assume that the conformation of peptidomimetics derived from the sequence of the native SNAP-25 substrate around the scissile bond should resemble that of SNAP-25 in the substrate:enzyme complex. However, and of interest from a general structural point of view, comparison of both BoNT/A LC complexes (i.e., wild-type BoNT/A LC: I1 and BoNT/A LC[E224Q,Y366F]:SNAP-25) shows that the closely SNAP-25-related I1 assumes a compact, α-helical conformation that maximizes its packing interactions with the active site, while the corresponding segment in SNAP-25 (i.e., QRATKML) adopts an extended, β stranded conformation (Figure 7). This striking observation suggests that the intrinsic plasticity of active sites in proteases, which can be a limiting factor in the development of specific inhibitors, can actually be overcome by designing peptidomimetics whose structural conformation differs significantly from the cognate substrate. Thus, although the backbones of both, I1 and SNAP-25, have the same directionality (i.e., N to C terminus) relative to the active site of the enzyme, I1, by virtue of its novel backbone orientation, is able to induce pockets in the active site (described above) that are not induced by SNAP-25. As an additional result of this unexpected new conformation of I1, the P5′ Met is clearly unable to establish the β-exosite contacts with BoNT/A LC residues Y250 and F369 observed for the corresponding SNAP-25 M202 residue in the BoNT/A LC[E224Q,Y366F]:SNAP-25 complex (Breidenbach and Brunger, 2004) (Figure 7B). Furthermore, the backbone and side chains of BoNT/A LC residues Q67 and V68 are displaced by the presence of the C-terminal Leu residue in the I1 peptide, relative to the SNAP-25-bound form of BoNT/A LC [E224Q,Y366F] (Figure 7B). Thus, these two residues are positioned toward a more solvent-exposed region in the I1-bound

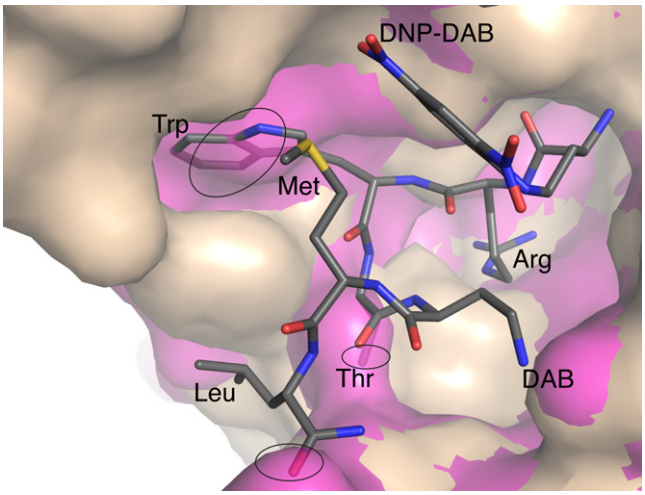

Figure 4. Induced-Fit Binding of I1 to the BoNT/A Active Site
View of the binding cleft of the BoNT/A LC (tan surface) in complex with inhibitor I1 (gray sticks). Inhibitor residues are indicated by their three-letter amino acid code, with the exception of residues P1 and P4′ (DNP-DAB and DAB, respectively). The induced binding pocket is evidenced by the steric clashes between the apo BoNT/A LC surface (magenta) with inhibitor residues Trp, Thr, and Leu upon superposition (translucent overlaps indicated by the black ovals).

form, whereas in the SNAP-25-bound form of the protease they point to the entrance of the binding site, in which case they would clash with the Leu residue in I1. Overall, these findings reveal a very different binding mode for SNAP-25 substrate and I1 inhibitor. Furthermore, SAR (Schmidt and Bostian, 1997; Schmidt et al., 1998) are also at odds with the assumption of a similar binding mode (Table 2). For example, as discussed above, substitution of Ala (SNAP-25 sequence) with Trp in the P2′ position of the inhibitor significantly increases its K_i.

The P1′ Arg of I1 probably binds to the native S1′ site on BoNT/A LC since the coordination of the scissile carbonyl oxygen in our structure is consistent with the catalysis mechanism (Figures 5A–C). Furthermore, the Arg side chain contacts with D370 and F194 observed in our structure have also been reported for the BoNT/A LC:ArgHX complex(Silvaggi et al., 2007). Therefore, these two observations, together with mutagenesis data that demonstrate the requirement of the BoNT/A LC for an Arg residue in the P1′ position (Schmidt et al., 1998), support the notion that the binding site for the P1′ I1 residue corresponds to the S1′ site in BoNT/A LC. The SNAP-25 contacts at the BoNT/A LC exosites favor the extended conformation of the substrate chain in the vicinity of the active site (i.e., the SNAP-25 scissile bond), which otherwise would collapse into a compact, nonhydrolyzable structure. The extended conformation of BoNT/A LC bound SNAP-25 ensures that the backbone amide group in the P1′ position, and not the P1 amide group (as observed for the I1 inhibitor), is in a competent orientation for attack by the catalytic water in the protease, resulting in the cleavage of the peptide bond.

A cocrystal structure of BoNT/A LC with a weakly inhibiting (K_i = 1.9 μM) heptapeptide, N-Ac-CRATKML, has been recently reported (Silvaggi et al., 2008). In this complex, the Cys $S\gamma$ atom directly coordinates the Zn^{2+} in the protease active site. Although the backbone secondary structure and directionality of this peptide is somewhat similar to that of I1, the direct coordination to the Zn^{2+} results in very different peptide:protein interactions. For the N-Ac-CRATKML peptide, the N-terminal acetyl group partially occupies the S1′ site in the enzyme, resulting in an altered placement of the P1′ Arg residue, which no longer makes the salt bridge contact with D370, observed for I1. In addition, the P2′ Ala residue in the N-Ac-CRATKML peptide lacks many of the interactions of the corresponding Trp sidechain in I1, explaining in part the superior potency of I1 versus N-Ac-CRATKML. For example, the small methyl side chain of the Ala residue of N-Ac-CRATKML can only form limited hydrophobic

Table 2. Inhibitor and Inhibition (K_i) Data

Inhibitor	Inhibitor Sequence[a,b,c]							K_i (μM)	Std. Dev.
	P1	P1′	P2′	P3′	P4′	P5′	P6′		
I2	Q	R	A	T	K	M	L	6.5	0.19
I3	3-Phenylpropanoyl-	R	A	T	K	M	L	>200	
I4	N-Acetyl-F	R	A	T	K	M	L	>200	
I5	[D]F	R	A	T	K	M	L	>200	
I6	F	R	A	T	K	M	L	8.3	0.79
I7	G	R	A	T	K	M	L	3.3	0.12
I8	DNP-DAB	R	A	T	K	M	L	0.98	0.12
I9	DNP-DAB	R	BZA	T	K	M	L	0.094	0.015
I10	DNP-DAB	R	BZA	T	DAB	M	L	0.05	0.0073
I11	DNP-DAB	R	F	T	K	M	L	0.32	0.021
I12	DNP-DAB	R	W	T	ORN	M	L	0.1	0.023
I13	DNP-DAB	R	W	T	DAP	M	L	0.39	0.01
I1	DNP-DAB	R	W	T	DAB	M	L	0.041	0.0084

[a] All peptides have a free amino group at the N terminus, unless noted otherwise, and the C terminus is amidated.
[b] Nonstandard abbreviations: DNP-DAB, 4-(2,4-dinitrophenylamino)-2-amino-butanoic acid; ORN, ornithine; DAB, 2,4-diaminobutanoic acid; DAP, 2,3-diaminopropanoic acid; BZA, benzothien-3-yl-alanine.
[c] All amino acids are the [L] stereoisomer unless noted otherwise.

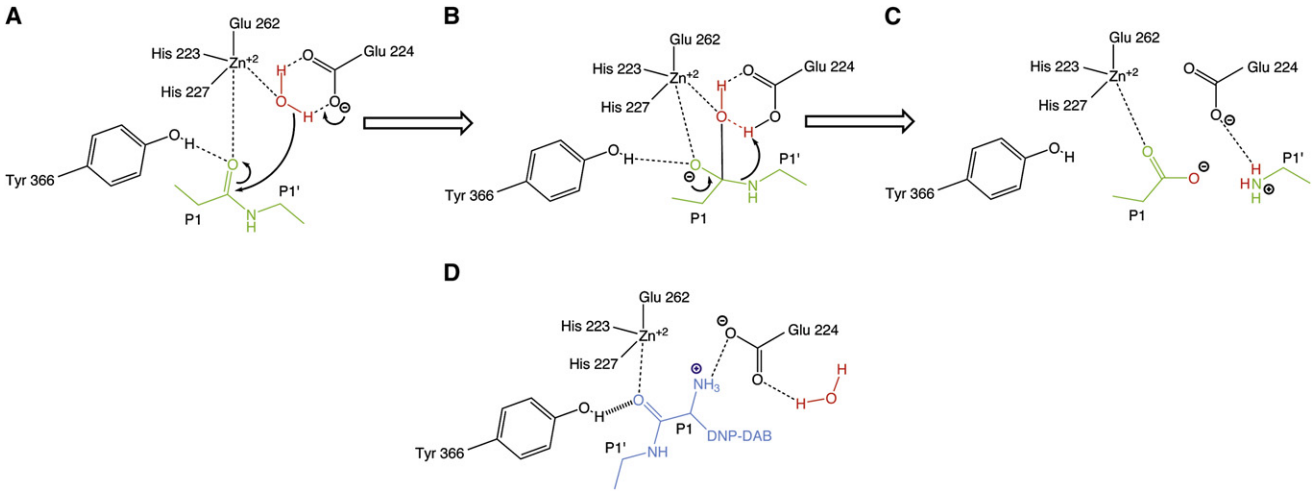

Figure 5. Mechanism of Inhibition by I1

(A–C) Schematic representation of a model for BoNT/A LC-catalyzed hydrolysis of SNAP-25. Atoms, bonds, and residue labels of the BoNT/A LC, SNAP-25 substrate, and the water molecules are shown in black, green, and red, respectively. Details are provided in the main text.

(D) Schematic representation of the interactions of the I1 inhibitor with residues in the active site of the BoNT/A LC. Atoms, bonds, and residue labels of the I1 inhibitor are shown in blue.

contacts with the side chain of V258. By contrast, the analogous Trp side chain of I1 forms highly favorable π-stacking between its phenyl portion of the indole and the side chain of Phe369. This interaction occurs in combination with favorable hydrophobic contacts formed with side chain of Leu256 for this same substituent. *Anti* to this interaction, the phenyl portion of the I1 Trp indole also forms favorable hydrophobic contacts with the side chain of L367. These contacts are further stabilized by favorable acid-base interactions between the side chain NH of Trp and the backbone carbonyl of E257, and hydrophobic complementarity between I1 Trp Cβ, Cγ, and Cδ1 atoms with aromatic atoms of Y366. As highlighted by the marked differences between the conformations of this region for the N-Ac-CRATKML:BoNT/A LC and I1:BoNT/A LC structures, these key interactions induced by I1 Trp provide novel, specific details to exploit in future structure-based discovery and design investigations.

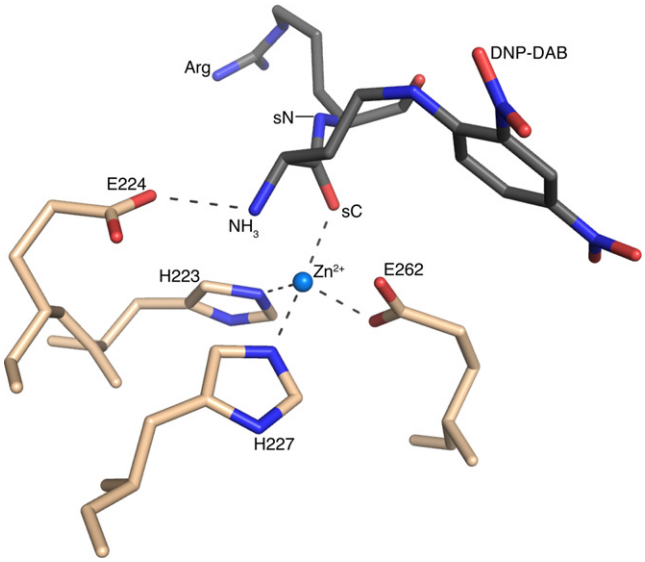

Figure 6. Inhibitory Interactions of I1

Coordination of the zinc ion in the presence of bound I1 (gray sticks). The putative scissile carbonyl oxygen (sC), scissile amide nitrogen (sN), and the terminal NH_3 group of I1 are labeled. BoNT/A LC residues are shown as tan sticks. The side chains of Arg and DNP-DAB in I1 are also labeled. Interactions are represented as dashes. N, C, and O atoms are color-coded in blue, tan/gray, and red, respectively. The zinc ion is represented by a light blue sphere.

Implications for BoNT/A LC Inhibitor Development

Our cocrystal provides a new paradigm for peptidomimetic inhibitor binding in the BoNT/A LC substrate cleft and rationalizes the SAR of related derivatives. This can serve as the platform for designing more-potent analogs with therapeutic viability. For example, the helical nature of the I1 conformation implies that peptidic cyclization in an isosteric manner would simultaneously provide affinity and a feasible bioavailability component for a peptide structure. The hydrolyzable components such as peptide bonds could be systematically replaced with nonhydrolyzable isosteres.

Table 3. Specificity of I1 Inhibition

Protease	Substrate	Substrate Concentration (μM)	% Inhibition
BoNT/A	SNAP-25, residues 187–203	400	>90
BoNT/B	VAMP residues 1–94	20	0
BoNT/D	VAMP residues 1–94	20	0
BoNT/E	SNAP-25, residues 1–206	20	0
BoNT/F	VAMP residues 1–94	20	0
Thermolysin	Synthetic peptide[a]	500	0

The inhibitor concentration was 4 μM.

[a] The sequence of the synthetic peptide was KLSELDDRADALQAGAS.

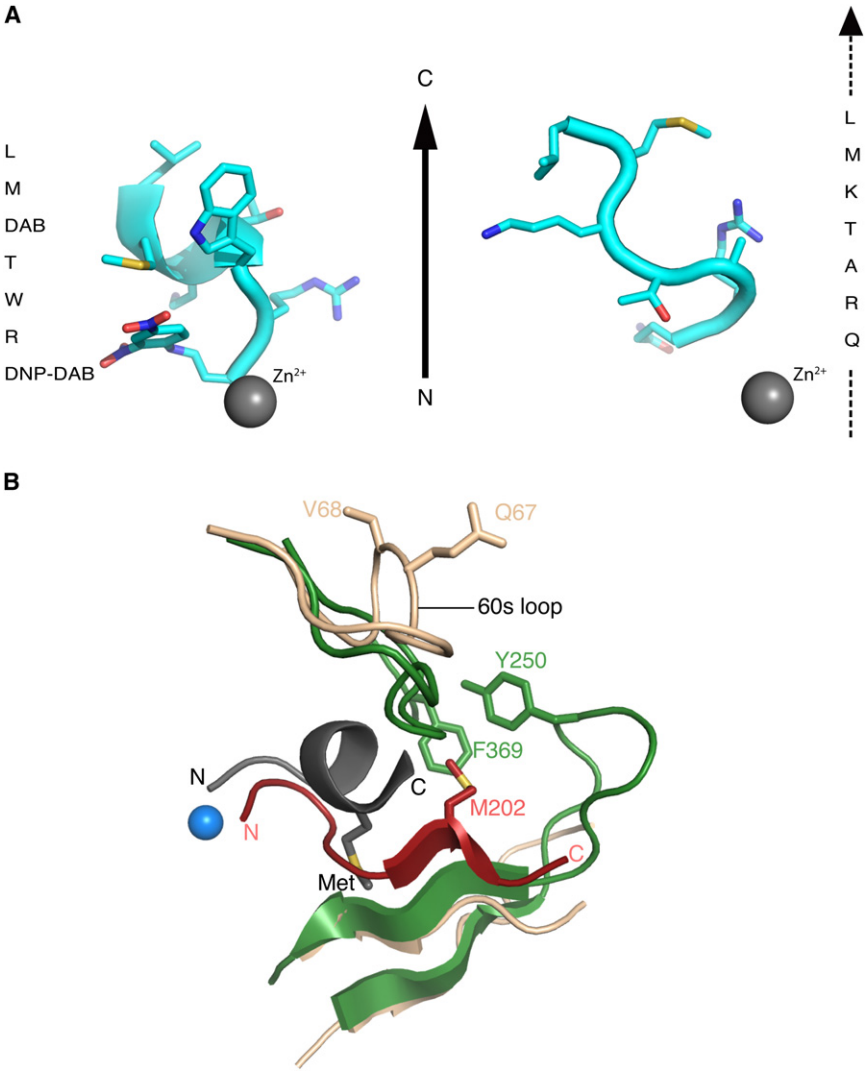

Figure 7. Comparison of the I1 Conformation with that of SNAP-25

(A) Cartoon representation of the backbone of BoNT/A LC-bound inhibitor I1 (left) and the Q197-L203 fragment in BoNT/A LC-bound SNAP-25 (right). The backbones of the corresponding BoNT/A LC structures were superimposed to produce the shown orientations of I1 and the SNAP-25 fragment. For clarity, the corresponding BoNT/A LC structures are not shown. The identity of the residues in both molecules is indicated by their one-letter code, with the exception of residues DAB and DNP-DAB in I1. Side chains of all residues are shown as sticks. N, C, O, and S atoms are colored in blue, cyan, red, and yellow, respectively. The Zn^{2+} is displayed as a gray sphere. Both backbones display the same N-to-C terminus directionality indicated by the solid vertical arrow. The dashed vertical line indicates the presence of additional SNAP-25 residues on both ends of the Q197-L203 fragment, which have been omitted for clarity.

(B) Cartoon representation of the superposition of the BoNT/A LC complexes with I1 and SNAP-25 (tan and green cartoons, respectively). The cartoon representation of I1 and the QRATKML sequence in SNAP-25 are shown in gray and red, respectively, with their N and C termini appropriately indicated. Selected residues of the BoNT/A LC forming part of the reported β-exosite are shown as green sticks. Residues in the 60 loop of BoNT/A LC undergoing I1-induced conformational changes are shown as tan sticks. The side chains of the Met residues in I1 and SNAP-25 are shown as sticks, with the sulfur atom colored yellow. The Zn^{2+} is shown as a light blue sphere.

The cocrystal structure suggests modifications of I1 to further enhance its potency. For example, removal or replacement of the P6′ Leu with an amphipathic bioisoteric moiety such as a morpholino group would be expected to reduce the entropic penalty associated with this hydrophobic residue so close to the solvent-exposed area. Further inspection of the I1 binding site reveals additional potential binding pockets that might be available for other chemical substituents to be included in future inhibitors. In particular, unexploited hydrophobic patches such as the one formed by the I161 and F194 side chains or that defined by the side chains of residues F196, T215, and V219, provide areas where new hydrophobic functional groups could be incorporated to increase inhibitor:enzyme hydrophobic binding. Superposition of these two patches in the apo and bound forms of the enzyme suggest a high degree of rigidity for these hydrophobic patch forming residues (RMSD < 0.15 Å). Finally, the hydrophobic pocket formed around the P2′ Trp is an important new site for exploiting additional contacts that could further stabilize binding in this induced pocket.

In addition to strategies for the design of improved peptide-based BoNT inhibitors, the α-helical conformation of bound I1 and its chemical contacts can be used as a template for design of small molecule nonpeptidic inhibitors. This approach would involve using the relative geometries and distances of the key substituents of the inhibitor to generate three-dimensional search queries for database mining.

In summary, the BoNT/A LC:I1 complex reveals a binding conformation for BoNT inhibitors in the catalytic cleft of the BoNTA/LC that is very different from that of SNAP-25 substrate. A key feature of this new binding mode is the induction of new binding pockets in the active site of BoNT/A LC. Our structure reveals that the basis for inhibition of BoNT/A LC catalytic activity by I1 involves the displacement of the catalytic water molecule and interactions with the side chain of E224 in the enzyme active site. The BoNT/A LC residues observed to interact with the P1′ Arg in I1 likely correspond to the native S1′ site of the enzyme. The structure of the BoNT/A LC:I1 complex and the observation of new induced binding pockets is a starting point for the rational design of more potent peptidomimetic inhibitors that are active in the sub nM range, and provides a new framework for the development of nonpeptidic, non-zinc-coordinating, small molecule inhibitors. Finally, the high specificity displayed by I1 against

BoNT/A (Table 3) indicates that compounds designed to mimic the interactions described for this inhibitor are likely to display the same specificity, and therefore, little or no side effects on related protease systems, a feature highly desirable in the development of therapeutic drugs.

EXPERIMENTAL PROCEDURES

Protein Expression and Purification

Details of the bacterial expression and purification of the active form of wild-type BoNT/A LC used in this study have been previously described (Breidenbach and Brunger, 2004). Solutions of wild-type BoNTA-LC containing 20 mM HEPES (pH 7.4) were adjusted to a final 50 μM protein concentration.

Crystallization and Data Collection

Crystals were obtained by using the hanging drop vapor diffusion method at 20°C. Briefly, 3 μl of a 50 μM protein stock were mixed with 1 μl of the mother liquor containing 0.1X PEG MME 2000, 5 mM $NiCl_2$, and 100 mM HEPES (pH 7.8). A layer of a 1:1 mixture of parafin:silicon oil was poured onto the mother liquor present in the well. Crystals appeared after approximately five days of incubation. In order to achieve the binding of the I1 inhibitor to BoNT/A LC in a complex, the crystals generated above were soaked in 3 μl drops of a 1 mM I1 water solution for 5 min at RT. Then, they were further transferred into a 3 μl drop of a 3 mM I1 solution. Five minutes after this second soak, the crystals were directly transferred into a cryo-solution containing 25% (v/v) glycerol, 0.1 X PEGMME 2000, 5 mM $NiCl_2$, and 100 mM HEPES (pH 7.8), and then were frozen in liquid nitrogen. The diffraction data were collected at beamline 9.1 of the SSRL (Stanford Synchrotron Radiation Laboratory) at a wavelength of 1 Å and at a temperature of 100°K. The soaked crystals belonged to the $P2_12_12$ space group. Integration, indexing, and scaling of the diffraction data was performed using the HKL2000 suite of programs (Otwinowski and Minor, 1997).

Structure Determination and Refinement of the Wild-Type BoNT/A LC

The coordinates in the 2ISG pdb file were used as the template for solving the structure of the apo form of wild-type BoNT/A LC using the PHASER module in CCP4i (McCoy et al., 2005). The calculated phases from the molecular replacement step allowed for the generation of a σ_A-weighted mF_o-DF_c electron density that unambiguously indicated the presence of the Zn and the Ni ions. Cross-validation was performed by excluding 5% of the diffraction data throughout the entire refinement process. After a few refinement cycles using Phenix (Adams et al., 2002), water molecules were added, and further refinement calculations were performed, alternated with manual modeling in Coot (Emsley and Cowtan, 2004). The quality of the final structure was assessed by using MolProbity (Davis et al., 2007). Ramachandran analysis showed that the apo BoNT/A LC had 96.4% residues in the favored region with only 0.26% outliers.

The Ni ion present in this crystal form of BoNT/A LC is coordinated by the side chain amino group of K272 and the NE2 atom from H269 from one BoNT/A LC molecule, and by the ND2 atom in the side chain amide group of N410 from a BoNT/A LC molecule in the neighboring asymmetric unit, as well as by three water molecules. Compared to other reported crystal structures of the BoNT/A LC that were obtained in the absence of Ni, this ion causes the side chains of K272 and H269 to reorient into closer proximity. Nevertheless, the backbone atoms of the H269-K272 segment remain, overall, in the same orientation in all BoNT/A LC structures. More importantly, these residues, and those in the vicinity, are distant from the active site and do not participate in a direct interactions with the I1 inhibitor or its interacting residues.

Structure Determination and Refinement of the Wild-Type BoNT/A LC-I1 Complex

The coordinates in the 1XTF pdb file were used as the search model to determine the structure of the wild-type BoNT/A LC-I1 complex by molecular replacement. The σ_A-weighted mF_o-DF_c electron density map clearly indicated the presence of I1 in the vicinity of the active site (Figure 1C). The coordinates of the I1 inhibitor were then added to those of the BoNT/A LC in the structure of the complex using Coot. Final refinement and modeling was performed as with the apo form of the BoNT/A LC. The quality of the final structure was assessed by using MolProbity. Ramachandran analysis showed that the BoNT/A LC:I1 structure had 97.7% residues in the favored region with no outliers.

Inhibitor Synthesis

Peptides and peptidomimetics were synthesized with a model 431A Peptide Synthesizer from Applied Biosystems (Foster City, CA). Reagents and amino acid intermediates were obtained from Applied Biosystems (Foster City, CA), Bachem (King of Prussia, PA), and from EMD Biochemicals (La Jolla, CA). All peptides were C-terminal amides. Inhibitors were purified by reverse-phase HPLC with gradients of dilute trifluoroacetic acid and acetonitrile using equipment from Waters Associates (Milford, MA). Molecular weights of the inhibitors were confirmed by mass spectrometry.

Determination of K_i Values

The protease activity of the BoNT/A LC in the presence of various concentrations of inhibitors was determined as described previously for the holotoxin (Schmidt and Bostian, 1997; Schmidt et al., 1998) with minor modifications. To determine initial hydrolysis rates, assays were incubated at 37°C for various times, depending on substrate and inhibitor concentrations, such that less than 10% of the substrate was hydrolyzed. K_i values of inhibitors were then calculated from fractional inhibition determinations using the equation:

$K_i = [I] - (F)[I] / (F)(1 + ([S] / K_m))$, where [I] and [S] are the concentrations of inhibitor and substrate, respectively, and F is fractional inhibition (Segel, 1975). Values are averages of at least three independent determinations, each in triplicate. As an inherent property of the inhibitor, K_i is independent of the substrate used to determine it: $Ki = [E][I] / [EI]$. Nevertheless, the K_i for I1 in kinetic assays with full-length SNAP-25 substrate was also determined and found to be the same as for the method used by Schmidt et al. (1998). Measured K_i values against BoNT/A LC and holotoxin BoNT/A are very similar for peptide analogs similar to I1, so all inhibition assays were performed only against BoNT/A LC.

Specificity of I1 Inhibition

The protease activity of various BoNT serotypes and thermolysin in the presence of I1 inhibitor was determined as described previously (Schmidt and Bostian, 1997). BoNT/B LC was obtained from Leonard Smith (United States Army Medical Research Institute of Infectious Diseases, Frederick, MD). BoNT/F LC was provided by S. Swaminathan (Brookhaven National Laboratory, Upton, NY). BoNT/E LC was purchased from BB Tech (Dartmouth, MA), and thermolysin was purchased from Sigma-Aldrich (St. Louis, MO). The gene for BoNT/D LC chain was provided by Raymond Stevens (Scripps Research Institute, La Jolla, CA). It was expressed and purified in the laboratory of J.J.S. (unpublished procedure). Recombinant VAMP (residues 1–94) and full-length SNAP25 were cloned, expressed, and purified in the laboratory of JJS (unpublished procedures). The peptide substrate for thermolysin was produced with a model 431A peptide synthesizer from Applied Biosystems (Foster City, CA), using chemicals and protocols obtained from the same manufacturer. The peptide was purified by reverse-phase HPLC using a gradient of acetonitrile in 0.1% trifluoroacetic acid (TFA).

The figures were prepared using PyMol (http://www.pymol.org).

ACCESSION NUMBERS

The coordinates and structure factors have been deposited into PDB (ID 3DSE for apo BoNT/A LC and PDB ID 3DS9 for the BoNT/A LC:I1 complex).

ACKNOWLEDGMENTS

SSRL is a national user facility operated by Stanford University on behalf of the US Department of Energy (Office of Basic Energy Sciences). The SSRL Structural Molecular Biology Program is supported by the Department of Energy (Office of Biological and Environmental Research), and by the National Institutes of Health (National Center for Research Resources, Biomedical Technology Program), and the National Institute of General Medical Sciences. This work was supported by the Department of Defense (proposal number

3.10024_06_RD_B to A.T.B.) and by the Defense Threat Reduction Agency (proposal number 3.10023_07_RD_B to J.J.S.). Opinions, interpretations, conclusions, and recommendations are those of the authors and are not necessarily endorsed by the US Army. This project has been funded in whole or in part with federal funds from the National Cancer Institute, National Institutes of Health, under contract N01-CO-12400. The content of this publication does not necessarily reflect the views or policies of the Department of Health and Human Services, nor does mention of trade names, commercial products, or organizations imply endorsement by the U.S. Government. This research was supported in part by the Developmental Therapeutics Program in the Division of Cancer Treatment and Diagnosis of the National Cancer Institute.

Received: June 20, 2008
Revised: July 11, 2008
Accepted: July 13, 2008
Published: October 7, 2008

REFERENCES

Adams, P.D., Grosse-Kunstleve, R.W., Hung, L.W., Ioerger, T.R., McCoy, A.J., Moriarty, N.W., Read, R.J., Sacchettini, J.C., Sauter, N.K., and Terwilliger, T.C. (2002). PHENIX: building new software for automated crystallographic structure determination. Acta Crystallogr. D Biol. Crystallogr. *58*, 1948–1954.

Agarwal, R., Eswaramoorthy, S., Kumaran, D., Binz, T., and Swaminathan, S. (2004). Structural analysis of botulinum neurotoxin type E catalytic domain and its mutant Glu212→Gln reveals the pivotal role of the Glu212 carboxylate in the catalytic pathway. Biochemistry *43*, 6637–6644.

Binz, T., Bade, S., Rummel, A., Kollewe, A., and Alves, J. (2002). Arg(362) and Tyr(365) of the botulinum neurotoxin type a light chain are involved in transition state stabilization. Biochemistry *41*, 1717–1723.

Blasi, J., Chapman, E.R., Link, E., Binz, T., Yamasaki, S., De Camilli, P., Sudhof, T.C., Niemann, H., and Jahn, R. (1993a). Botulinum neurotoxin A selectively cleaves the synaptic protein SNAP-25. Nature *365*, 160–163.

Blasi, J., Chapman, E.R., Yamasaki, S., Binz, T., Niemann, H., and Jahn, R. (1993b). Botulinum neurotoxin C1 blocks neurotransmitter release by means of cleaving HPC-1/syntaxin. EMBO J. *12*, 4821–4828.

Boldt, G.E., Kennedy, J.P., and Janda, K.D. (2006). Identification of a potent botulinum neurotoxin a protease inhibitor using in situ lead identification chemistry. Org. Lett. *8*, 1729–1732.

Breidenbach, M.A., and Brunger, A.T. (2004). Substrate recognition strategy for botulinum neurotoxin serotype A. Nature *432*, 925–929.

Burnett, J.C., Ruthel, G., Stegmann, C.M., Panchal, R.G., Nguyen, T.L., Hermone, A.R., Stafford, R.G., Lane, D.J., Kenny, T.A., McGrath, C.F., et al. (2007). Inhibition of metalloprotease botulinum serotype A from a pseudo-peptide binding mode to a small molecule that is active in primary neurons. J. Biol. Chem. *282*, 5004–5014.

Davis, I.W., Leaver-Fay, A., Chen, V.B., Block, J.N., Kapral, G.J., Wang, X., Murray, L.W., Arendall, W.B., 3rd, Snoeyink, J., Richardson, J.S., and Richardson, D.C. (2007). MolProbity: all-atom contacts and structure validation for proteins and nucleic acids. Nucleic Acids Res. *35*, W375–W383.

Emsley, P., and Cowtan, K. (2004). Coot: model-building tools for molecular graphics. Acta Crystallogr. D Biol. Crystallogr. *60*, 2126–2132.

Fu, Z., Chen, S., Baldwin, M.R., Boldt, G.E., Crawford, A., Janda, K.D., Barbieri, J.T., and Kim, J.J. (2006). Light chain of botulinum neurotoxin serotype A: structural resolution of a catalytic intermediate. Biochemistry *45*, 8903–8911.

Josko, D. (2004). Botulin toxin: a weapon in terrorism. Clin. Lab. Sci. *17*, 30–34.

Kukreja, R., and Singh, B. (2005). Biologically active novel conformational state of botulinum, the most poisonous poison. J. Biol. Chem. *280*, 39346–39352.

Kumaran, D., Rawat, R., Ludivico, M.L., Ahmed, S.A., and Swaminathan, S. (2008). Structure- and substrate-based inhibitor design for *Clostridium botulinum* neurotoxin serotype A. J Biol. Chem. *283*, 18883–18891.

Lacy, D.B., Tepp, W., Cohen, A.C., DasGupta, B.R., and Stevens, R.C. (1998). Crystal structure of botulinum neurotoxin type A and implications for toxicity. Nat. Struct. Biol. *5*, 898–902.

Li, L., Binz, T., Niemann, H., and Singh, B.R. (2000). Probing the mechanistic role of glutamate residue in the zinc-binding motif of type A botulinum neurotoxin light chain. Biochemistry *39*, 2399–2405.

McCoy, A.J., Grosse-Kunstleve, R.W., Storoni, L.C., and Read, R.J. (2005). Likelihood-enhanced fast translation functions. Acta Crystallogr. D Biol. Crystallogr. *61*, 458–464.

Otwinowski, Z., and Minor, W. (1997). Processing of X-ray diffraction data collected in oscillation mode. Methods Enzymol. *276*, 307–326.

Rao, B.G. (2005). Recent developments in the design of specific Matrix Metalloproteinase inhibitors aided by structural and computational studies. Curr. Pharm. Des. *11*, 295–322.

Schiavo, G., Benfenati, F., Poulain, B., Rossetto, O., Polverino de Laureto, P., DasGupta, B.R., and Montecucco, C. (1992). Tetanus and botulinum-B neurotoxins block neurotransmitter release by proteolytic cleavage of synaptobrevin. Nature *359*, 832–835.

Schmidt, J.J., and Bostian, K.A. (1997). Endoproteinase activity of type A botulinum neurotoxin: substrate requirements and activation by serum albumin. J. Protein Chem. *16*, 19–26.

Schmidt, J.J., Stafford, R.G., and Bostian, K.A. (1998). Type A botulinum neurotoxin proteolytic activity: development of competitive inhibitors and implications for substrate specificity at the S1′ binding subsite. FEBS Lett. *435*, 61–64.

Segel, I.H. (1975). Enzyme kinetics: behavior and analysis of rapid equilibrium and steady state enzyme systems (New York: Wiley).

Silvaggi, N.R., Boldt, G.E., Hixon, M.S., Kennedy, J.P., Tzipori, S., Janda, K.D., and Allen, K.N. (2007). Structures of *Clostridium botulinum* neurotoxin serotype A light chain complexed with small-molecule inhibitors highlight active-site flexibility. Chem. Biol. *14*, 533–542.

Silvaggi, N.R., Wilson, D., Tzipori, S., and Allen, K.N. (2008). Catalytic features of the botulinum neurotoxin A light chain revealed by high resolution structure of an inhibitory peptide complex. Biochemistry *47*, 5736–5745.

Suzuki, T., and Miyata, N. (2005). Non-hydroxamate histone deacetylase inhibitors. Curr. Med. Chem. *12*, 2867–2880.

Swaminathan, S., Eswaramoorthy, S., and Kumaran, D. (2004). Structure and enzymatic activity of botulinum neurotoxins. Mov. Disord. *19* (*Suppl 8*), S17–S22.